INFORMATION TO USERS

This manuscript has been reproduced from the microfilm master. UMI films the text directly from the original or copy submitted. Thus, some thesis and dissertation copies are in typewriter face, while others may be from any type of computer printer.

The quality of this reproduction is dependent upon the quality of the copy submitted. Broken or indistinct print, colored or poor quality illustrations and photographs, print bleedthrough, substandard margins, and improper alignment can adversely affect reproduction.

In the unlikely event that the author did not send UMI a complete manuscript and there are missing pages, these will be noted. Also, if unauthorized copyright material had to be removed, a note will indicate the deletion.

Oversize materials (e.g., maps, drawings, charts) are reproduced by sectioning the original, beginning at the upper left-hand corner and continuing from left to right in equal sections with small overlaps. Each original is also photographed in one exposure and is included in reduced form at the back of the book.

Photographs included in the original manuscript have been reproduced xerographically in this copy. Higher quality 6" x 9" black and white photographic prints are available for any photographs or illustrations appearing in this copy for an additional charge. Contact UMI directly to order.

UMI

A Bell & Howell Information Company
300 North Zeeb Road, Ann Arbor MI 48106-1346 USA
313/761-4700 800/521-0600

α6β1 AND α6β4 INTEGRIN EXPRESSION AND THE VASCULARIZATION OF HUMAN PROSTATE TUMOR XENOGRAFTS

by

John Richard McCandless, Jr.

A Thesis Submitted to the Faculty of the

DEPARTMENT OF BIOCHEMISTRY

In Partial Fulfillment of the Requirements
For the Degree of

MASTER OF SCIENCE

WITH A MAJOR IN GENERAL BIOLOGY

In the Graduate College

UNIVERSITY OF ARIZONA

1 9 9 7

STATEMENT BY AUTHOR

This thesis has been submitted in partial fulfillment of requirements for an advanced degree at The University of Arizona and is deposited in the University Library to be made available to borrowers under rules of the Library.

Brief quotations from this thesis are allowable without special permission, provided that accurate acknowledgment of source is made. Requests for permission for extended quotation from or reproduction of this manuscript in whole or in part may be granted by the head of the major department or the Dean of the Graduate College when in his or her judgment the proposed use of the material is in the interests of scholarship. In all other instances, however, permission must be obtained from the author.

SIGNED: 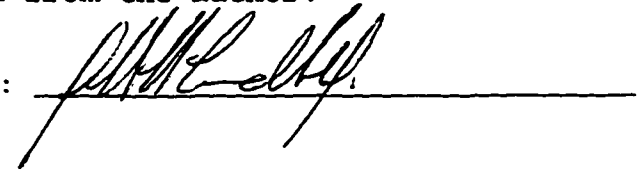

APPROVAL BY THESIS DIRECTOR

This thesis has been approved on the date shown below:

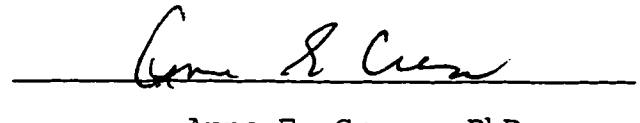 4/28/97

Anne E. Cress, PhD — Date

Professor of Radiation Oncology

ACKNOWLEDGEMENTS

I would like to express my deep gratitude to Dr. Anne E. Cress, my thesis advisor, for providing me with the opportunity to conduct this research. I am especially appreciative of the many hours she spent in guiding the development of my understanding of the nature of scientific research. I would also like to thank the other members of my thesis committee, Dr. Ray B. Nagle and Dr. Stuart K. Williams, for their guidance, assistance, and the use of their laboratory facilities.

I owe a deep debt of gratitude to Kathy McDaniel for her help with all aspects of the project and for her proofreading abilities. I would also like to thank Virginia Clark, Karim Salam, Dennis Salzman, and Louis Breton of Dr. Nagle's and Dr. Williams' laboratories for their technical assistance and for the camaraderie the offered.

Finally, I would like to thank my son, Nick McCandless, for his remarkable patience throughout this effort.

DEDICATION

I would like to dedicate this work to the memory of my wife, Shelley McCandless, for all that she gave to me and for the good times and adventures we shared.

TABLE OF CONTENTS

TABLE OF CONTENTS - Continued

LIST OF FIGURES

LIST OF TABLES

ABSTRACT

Growth and metastasis of tumors appear to be dependent on the ability of tumor cells to recruit blood vessels. Integrins are a class of cell adhesion molecules that may have a role in angiogenesis. In this study the effect of the expression of two integrins, $\alpha 6\beta 1$ and $\alpha 6\beta 4$, on microvessel density in human prostate tumor xenografts in SCID mice was evaluated. Five methods (one-person count, two-person count, digital analysis of immunostained tissues, and digital analysis of vascular corrosion casts) were used to measure microvessel density. Results indicate that $\alpha 6$ integrin expression correlates negatively with tumor vessel density. and with tumor cell proliferation but not the extent of the tumor burden. $\beta 4$ integrin expression does not appear to affect tumor vessel density, tumor cell proliferation, nor tumor burden. Comparison of methods of quantitation suggest that computer-assisted vessel counting may offer advantages over optical counting or computer-assisted area measurement.

INTRODUCTION

The normal development, growth, and function of multicellular organisms depends on a very highly organized pattern of cellular growth, differentiation, interaction, and death. These processes in turn depend on genetically-determined molecular interactions both within and between the cells, and it is the study of these molecular events and their effects that lies at the foundation of the understanding of the physiology of multicellular organisms. Embryological studies of the molecular events associated with morphogenetic development have provided important insights into the mechanisms of intercellular interaction, as have studies of lymphocyte behavior in the inflammatory response. The study of cancer provides another system by which these biochemical events and their effects may be studied, for the behaviors of cancer cells reflect disruptions in the normal process of differentiation and gene expression and hence provide a way to associate molecular structure and function with the physiology of the cell. The study of the molecular events associated with cancer may lead to the improved diagnosis, treatment, and prevention of the disease in humans.

The Role of Angiogenesis in Tumor Development and Metastasis

The development of cancer has been considered to be a microevolutionary process, in which a subpopulation of otherwise normal cells acquires a competitive advantage over normal cells through mutation and the altered expression of certain gene products (Alberts, 1994). Cancer cells show an increased proliferative rate relative to the surrounding cells, and may acquire the potential to migrate through the surrounding tissues, enter the circulatory system, and invade distant tissues. Prevalent views suggest that this process of metastasis is a "marathon" in which only a tiny fraction of the primary tumors cells exhibit the necessary qualities that enable them to exit the primary tumor, migrate, and ultimately develop a tumor in a distant organ. (Liotta, 1992)

Recently, it has been recognized that interactions between cells within a tumor and between the cells of the tumor and the host tissue play a significant part in the development of the metastatic potential in a tumor cell line. (Rak, 1995) Thus, tumor growth and metastasis is a highly complex process that involves several levels of molecular interaction, and requires that the tumor cells not only be able to move through the extracellular matrix of the stroma but also to modify the tumor environment so as to provide conditions favorable to cell growth and replication.

The continued growth of a tumor has been found to be almost completely dependent on the ability of the tumor cells to recruit new vessels to the tumor (Brawer, 1994). Growth of a tumor beyond 3 mm^3 in volume without concurrent vascularization is rare (Folkman, 1987) due to the need for oxygen and nutrients by the cells within the tumor. Evidence suggests that angiogenesis is necessary but not thesole determinant of tumor growth (Folkman, 1995), as tumor cells that lack intrinsic growth potential will not proliferate despite suitable perfusion.

There is significant evidence that metastasis is also angiogenesis dependent (Fidler, 1994; Folkman, 1995). The most widely held view of metastasis requires that the metastatic cell enter the lymphatic/vascular system, migrate to the capillary bed of another organ, and extravasate into the distant tissue. These processes require that the tumor cell be capable of both proteolytic degradation of basement membranes and migration. Vascularization of a tumor improves the chances of tumor growth and thus increases the likelihood of the evolution of a metastatic subpopulation, while at the same time affording relatively easy access to the vascular system (Stracke, 1995). Tumor vessels may be particularly susceptible to invasion by tumor cells due to the fragmented, poorly organized nature of the basement membrane of newly-proliferating vessels (Weidner, 1995).

Metastasis to the lymph nodes may also be angiogenesis-dependent. Tumors rarely contain lymphatic vessels, but

lymph node metastases are not associated with prevascular tumors (Folkman, 1995). Much effort has been expended in recent years to associate the density of the tumor vasculature with cancer progression so as to develop a reliable prognostic tool for the assessment of various cancers (Weidner, 1995; Rak, 1995; Brawer, 1996).

Mechanisms of Angiogenesis

The mechanism by which a tumor recruits a new microcirculation appears to be dependent on paracrine interactions between the tumor cells and the endothelial cells that form the neovascular achitecture (Rak, 1995). Endothelial cells line blood vessels of all sizes and in capillaries, which consist of a single layer of endothelial cells surrounded by a basal lamina, the endothelial cells serve to control the flow of materials and leukocytes into and out of the circulatory system (Alberts, 1994). The growth of new vessels from pre-existing vessels, termed angiogenesis, is dependent on many mechanisms including the proliferation of endothelial cells. The development of a new blood vessel begins with the penetration of the basal lamina of the parent vessel by an endothelial cell, which is accomplished through the secretion of proteases such as collagenases and other matrix metalloproteinases (Murphy, 1993), followed by the formation of a prevascular bud as an endothelial cell of the parent vessel extends into the

surrounding tissue stroma.Subsequently, the endothelial cell divides and,through the development of spaces within and between the adjacent developing endothelial cells, a lumen is formed (Folkman, 1980). Continued growth of the neovessel may result from endothelial cell proliferation, migration, or remodelling (Fox, 1996).

The molecular interactions that mediate angiogenesis are complex. The most widely studied stimulators of angiogenesis are vascular permeability factor/vascular endothelial growth factor (VPF/VEGF) and members of the fibroblast growth factor (bFGF) family, especially bFGF (Folkman, 1995). By enhancing vascular permeability and the extravasation of plasma, VPF/VEGF promotes activation of the extrinsic coagulation pathway and the extravascular concentrations of various plasma-derived proteins, including thrombin (Senger, 1996b). This may alter the composition of the extracellular matrix, resulting in increased expression of adhesion molecules such as $\alpha v\beta 3$ integrin and its ligands (Senger, 1996b). The increased expression of VPF/VEGF and its receptors occurs with hypoxia, a common event in the growth of tumors that is associated with the increased interstitial pressure resulting from the lack of lymphatic penetration of the tumor (Liotta, 1992; Waleh, 1995). VPF/VEGF has been shown to be highly expressed by tumor cells (Zhang, 1995; Senger, 1996b). Endothelial cells found within tumors express VPF/VEGF, but not VPF/VEGF mRNA, suggesting that the endothelial cells are not producing VPF/VEGF (Weidner, 1995). The tumor

endothelial cells do show increased expression of VPF/VEGF receptors, and hence the neovascularization of the tumor may be directed by the VPF/VEGF activity of the tumor cells.

bFGF factor is known to increase vascular permeability (Senger, 1996b). bFGF has been shown to induce secretion of proteases by endothelial cells, promote endothelial cell proliferation, and regulate the expression of laminin-binding integrins on the endothelial cell surface to promote migration (Senger, 1996). Elevated levels of bFGF are found in the serum and urine of patients with a variety of cancers, although the mechanism by which these elevated levels are produced and sustained is unknown (Folkman, 1995). It is likely that VPF/VEGF and bFGF act synergistically to promote angiogenesis.

In addition to the stimulation by factors such as bFGF, VPF/VEGF and others, Folkman (1995) suggests other mechanisms of angiogenesis, including decreased expression of negative regulators, storage of heparin-binding growth factors and angiogenesis inhibitors on the cell surface or in the extracellular matrix, control of the shape of the endothelial cells which must elongate in order to form vesssels, loss of contact inhibition by pericytes and fibroblasts, loss of inhibition by various circulating and tumor-derived proteins, and the failure of tumor suppressor genes such as p53.

Integrins

Integrins are cell-surface heterodimeric glycoproteins found in nearly all tissues of the human body that mediate the interaction of the cytoskeleton and the extracellular matrix (Luscinskas, 1994). The subunits are known as α and β, and both present extracellular ligand-binding domains and short cytoplasmic domains linked by a short (20-30 amino acid residue) transmembrane domain (Cox,1994). There are currently fourteen α subunits and eight β subunits known that are organized into 20 distinct integrin heterodimers (Buck, 1995). Expression on the cell surface may be constitutive or may require *de novo* synthesis. Additionally, not all integrins are active when present in the plasma membrane, requiring activation (Cox, 1994). The cytoplasmic domain of the β subunit interacts with the cytoskeleton, and this interaction appears to determine the distribution of integrins within the cell (Buck, 1995).

The cytoplasmic domain of the α subunit appears to be involved in controlling the distribution of the integrin, regulating ligand binding, cell migration, and extracellular matrix remodeling, and controlling the behavior of the cell after ligand binding (Buck, 1995). The extracellular domains of both subunits function as receptors for ligands in the extracellular matrix, such as collagen, laminin, and fibronectin, that allow for cell migration and interaction

with the extracellular matrix, and for cell adhesion molecules to enable the binding of cells (Chammas, 1991). In addition to their role as adhesion molecules, integrins have also been shown have a role in signal transduction (Juliano, 1993).

The Role of Integrins in Prostate Carcinoma

The normal prostate gland consists of a layer of basal cells surrounded by a basal lamina. Interior to the basal cells is a layer of secretory columnar epithelium (Nagle, 1991). The attachment of the basal cells to laminin in the basal lamina occurs primarily through the integrins $\alpha6\beta1$ and $\alpha6\beta4$ (Nagle, 1995), although the integrins $\alpha2\beta1$, $\alpha3\beta1$, $\alpha4\beta1$, and $\alpha v\beta1$ are also present (Cress, 1995). $\alpha6\beta1$ integrin appears to be uniformly distributed on the cell membrane on the basolateral surface, while $\alpha6\beta4$ is associated with hemidesmosomes found at the interface of the basal cell and the basal lamina (Nagle, 1995).

The development of prostate cancer is accompanied by proliferation and progressive loss of differentiation by the lumenal cells lining the glands and ducts of the prostate (Cress, 1995). In later stages of tumor progression expression of the $\alpha2\beta1$, $\alpha3\beta1$, $\alpha4\beta1$, $\alpha v\beta1$, and $\alpha6\beta4$ integrins is decreased, while the expression of $\alpha6\beta1$ integrin is

maintained (Nagle, 1995) but appears to lack polarization (Witkowski, 1993).

Investigations of the migratory and invasive potential of two subpopulations of a human prostate cell line carcinoma in a SCID mouse model suggest that increased expression of α6β1 integrin is associated with a more invasive phenotype (Rabinovitz,1995). α6β1 and α6β4 integrins are expressed by certain endothelial cells (Luscinskas, 1994), which may account for the migration of malignant carcinoma cells along nerve tracts and meurovascular bundles (Cress, 1995). The tumor cells in this model showed continued expression of α6β1 integrin at the invasion front, as well as the ability to secrete altered forms of laminin that may contribute to the migratory potential (Cress, 1995).

The Role of Integrins in Angiogenesis

Various phenotypic changes that occur when an endothelial cell begins the formation of a new vessel. These changes include alterations in the levels of growth factors, proteases, protease inhibitors, adhesion molecules such as integrins, and other cell-surface receptors (Luscinskas, 1994), which enable the cell to modify the extracellular environment, migrate, and proliferate (Folkman,1987). Evidence from a number of investigators indicates that the integrins, in addition to their role as adhesion molecules,

play a significant part in signal transduction and influence cell function (Juliano, 1993; Luscinskas, 1994; Buck, 1995). Ligation of integrins has been shown to stimulate expression of proteases(Buck, 1995), The dependence of cell replication on adhesion to a substrate suggests that integrins may be involved in the initiation of mitosis (Folkman, 1995). VPF/VEGF has been shown to stimulate $\alpha v\beta 3$ integrin expression in endothelial cells, as well as its ligand osteopontin (OPN). The ligation of this integrin increases the migratory potential of the endothelial cells (Senger, 1996b). To date, however, the roles of $\alpha 6\beta 1$ and $\alpha 6\beta 4$ integrins in the signaling mechanisms involved with angiogenesis have not been determined.

Methods of Quantitation of Tumor Vasculature

In vivo methods of quantitating tumor angiogenesis are numerous and varied, and while some have gained wide acceptance, most have limitations. These methods are summarized in Table 1. Weidner (1991) has developed a method that relies on the counting of immunostained vessels in a 200-400x microscopic field of view. In this method, regions of high vessel density are first located at low magnification, and then the vessels are counted simultaneously by two observers. This method has been suggested to be an effective prognostic indicator of

Table 1: Methods of quantitation of tumor vasculature.

	Method	Reference
1.	Vessel counting in immunostained tissues by two observers	Weidner *et al*, 1991; Bosari *et al*, 1992
2.	Vessel counting in immunostained tissues using eyepiece graticle	Hollingsworth *et al*, 1995; Zhang *et al*, 1995
3.	Vessel counting in immunostained tissues using digital image analysis	Brawer *et al*, 1994
4.	Vessel area measurement in immunostained tissues using digital image analysis	Wakui *et al*, 1992; Kohlberger *et al*, 1996
5.	Scanning electron microscopy of vascular corrosion casts	Konerding *et al*, 1995; Less *et al* 1991

recurrence in breast cancer (Weidner, 1991; Bosari, 1992), prostate cancer (Weidner, 1993), lung cancer (Giatromanolaki, 1996), medullary thyroid cancer (Fontanini, 1996) and ovarian cancer (Hollingsworth, 1995). Limitations of this method include lack of uniformity in immunostaining due to variations in sensitivity of the antibody, cross-reactivity of the antibody, and observer bias in selecting "hot spots" of vascular activity and identifying vessels. Other investigators (Wakui, 1992; Brawer, 1994; Iwahana, 1996) have used computer-image processing techniques in combination with immunostaining in an attempt to address the problem of observer biases. Significantly, this method relies on random sampling of the tissue without regard to variations in vessel density and assesses the area of the vessels per unit of tumor area. Using such methods, Wakui (1992) and Brawer (1994) have found a high correlation between tumor microvessel density and pathologic stage in prostate carcinoma. Difficulties still exist with antibodies used for immunostaining, and selection of regions in the image representing *bona fide* vessels remains problematic. These techniques have also been applied to the study of tumor vasculature in animal model systems (Kibbey, 1992; Abe, 1996).

Hollingsworth (1995) describes a method of vessel quantitation in which four points in the focal plane of the tissue were randomly shifted with a mechanical stage. Coincidence of a stained endothelial cell and one of the

points was considered a hit, and the number of fields necessary to obtain 45 hits was counted.

In addition, a number of investigators (see Konerding, 1995, for a review) have used the technique of vascular corrosion casting, in which the vasculature of tumors is perfused with a plastic resin. Assays using conventional, confocal laser, and scanning electron microscopy have been performed on the resulting vascular casts. These have been used to describe the morpholgy of tumor vessels. This method also has limitations due to shrinkage of the casting material upon hardening, lack of complete perfusion due to resin viscosity, and distension of vessels due to excessive perfusion pressures (Kratky, 1989).

Hypothesis

Evidence suggests that the expression of integrins may influence the vascularization of tumors and hence the metastatic potential of tumor cells. This would suggest quantitative differences in the densities of the vascular tissues in tumors produced by tumor cells that exhibit differential expression of integrins. The SCID (severe combined immunodeficient) mouse model has been shown to be effective in the study of prostate carcinomas due to the directional orientation of the tumors on the mouse diaphragm and the availability of immunohistochemical methods of observation of the tumors (McCandless, 1997).

Intraperitoneal injection of the high and low α6 integrin expressers of the DU-145 prostate carcinoma cell line in SCID mice has indicated that tumors derived from low α6 integrin expressers (DU-L) tend to form larger, less invasive tumors as opposed to the generally smaller, more invasive tumors arising from the high α6 integrin expressers (DU-H; Rabinovitz, 1994). One possible explanation for the difference in tumor growth could be that the cell-line variants with a low level of expression of α6 (DU-L) produced tumors with a greater vascular density than tumors derived from cells with high α6 expression. This may allow the tumors derived from the low α6 cells to grow larger due to the improved supply of oxygen and nutrients.

Experimental Design

Five methods of quantitating microvessel density in tumors derived from metastatic human prostate carcinomas were used in order to thoroughly assess the effect of α6β1 and α6β4 integrin expression on tumor angiogenesis. These methods included optical counting of vessels in immunohistochemically stained tumors by two observers simultaneously ("two-person count"), optical counting of vessels in immunohistochemically-stained tumors by one observer ("one-person count"), computer assisted vessel

counting in immunohistochemically-stained tumors ("computer count"), computer-assisted measurement of total vessel area per unit tumor area in immunohistochemically-stained tumors ("computer area"), and computer-assisted measurement of total vessel area per unit tumor area in confocal laser microscope optical sections of vascular corrosion casts.

The first four of these methods involved immuno-histochemical staining of frozen diaphragm sections from SCID mice that had been injected with variants of the DU-145 human prostate carcinoma cell line. These sections were observed microscopically and the number of stained regions representing tumor vessels counted according to methods developed for the prognostication of metastatic potential in breast and prostate carcinoma (Weidener, 1991; Weidener, 1993). Digital images of these sections were then analyzed using image analysis software to determine the number of discrete stained regions and the total area of the stained regions.

The fifth method required the perfusion of the SCID mouse vasculature with a polymethyl methacrylate resin. This resin was known to fluoresce at 488 nm, one of the wavelengths used in confocal laser microscopy (Hossler, 1991), allowing for the use of a confocal microscope to quantitate both the number of vessels and the total vessel area in a field of view.

Dimensions of the tumor burden and the number of proliferating tumor cells per microscopic field were assesed

in order to investigate any possible correlation between tumor cell proliferation, tumor growth, tumor vascularization, and the expression of the α6β1 and α6β4 integrins. The correlation of results obtained from these methods allowed for the determination of variation in microvessel density among the high and low expressers of the α6 and β4 integrin subunits and may lead to interesting new lines of research regarding the role of the tumor vasculature in the interaction of the tumor cells and the host animal physiology. Additionally, the use of different methods of quantitation of the tumor vasculature will allow for a comparison of their relative effectiveness.

MATERIALS AND METHODS

Cell lines

The DU-145 human prostate carcinoma cell line was derived from a central nervous system metastasis of a primary prostate adenocarcinoma (American Type Culture Collection, Rockville, MD) (Mickey, 1980). Subpopulations of this cell line show differential expression of the integrin subunit α6, allowing for the selection of the DU-H cell line, which shows a four-fold increase in the level of expression of α6 integrin (primarily as α6β1) over the DU-L cell line (which expresses α6 integrin primarily as α6β4) by successive fluorescence-activated cell sorting (FACS) in which the cells were collected from the 2% 'tails' (Rabinovitz, 1995). DU-H cells were stably transfected with either a full-length β4 integrin construct or vector alone (Shaw, 1993). The cDNAs were subcloned into the pRc/CMV eukaryotic expression vector that uses the CMV promoter for expression (Invitrogen). The cells were transfected using 2 μg of cDNA vector and 20 μl of lipofectin reagent (Gibco, Grand Island, NY). Selection was achieved with DMEM medium containing 10% fetal bovine serum, 1% penicillin/streptomycin, supplemented with 400 μg/ml of G418 (Geneticin) and selected for high expression of the α6 and β4 integrins by FACS. All cell lines were maintained in

IDMEM (Gibco) with 10% fetal bovine serum (Gibco), penicillin (500 µg/ml), and streptomycin sulfate (500 µg/ml) at 37°C in humidified air with 5% CO_2. All populations tested negative for the presence of Mycoplasma and murine viruses.

SCID Mouse Model

The SCID mouse colony at the University of Arizona consists of BALB-c/B-17 mice (Jackson Laboratories, Bar Harbor, ME) maintained in a specific pathogen-free environment in compliance with USPHS guidelines governing the care and maintenance of animals. Male SCID mice 5-6 weeks old were inoculated intraperitoneally with 5 x 10^6 DU-L cells or 2.0 x 10^7 DU-H (xV or xB4) cells resuspended in 0.5 ml of phosphate-buffered saline (PBS, pH 7.0-7.4, prepared with monobasic and dibasic sodium phosphate) using a tuberculin syringe with a 25-gauge needle. The different number of cells was used to ensure a similar tumor burden in all mice, as previous observations have indicated that the DU-L cells have a higher tumor proliferative rate *in vivo* (Rabinovitz,1995). The mice were sacrificed by cervical dislocation 30 to 35 days after inoculation. The thoracic and abdominal cavities were opened separately, leaving the diaphragm intact, and the contents of the thoracic cavity were removed. A piece of filter paper was applied to the superior surface of the diaphragm to provide support while the diaphragm was removed,

usually with a rim of the attached ribcage, and placed on a dissecting surface of dental wax. Following weighing, the samples were divided using a razor blade. Portions of the samples were snap frozen in isopentane supercooled to -140°C in liquid nitrogen, embedded in OCT compound (Miles Laboratories), and stored at -70°C until used. Other portions were fixed for routine histology in 10% buffered formalin and embedded in paraffin. Thin wafers were oriented vertically in the embedding media to allow the preparation of transverse sections of the diaphragm showing developing tumors and the underlying tissues of the diaphragm.

Measurement of Tumor Vasculature: Immunohistochemical Methods

Immunohistochemistry. The antibody used for quantitation of the tumor vasculature was the monoclonal rat anti-mouse PECAM (platelet-endothelial cell adhesion molecule) antibody ab 390 (obtained as a gift from Dr. Clayton Buck, Wistar Institute, Philadelphia, PA) isolated by ammonium sulfate saturation from a rat hybridoma culture supernatant to a concentration of 0.6 mg/mL. The antibody was diluted in PBS-1% BSA (bovine serum albumin) to a concentration of 24 µg/mL and applied to acetone-fixed 4-µm frozen sections for 30 minutes in a humid chamber, then rinsed in PBS. Negative controls were prepared using PBS. After primary immunostaining, each specimen was incubated in a biotinylated

anti-rat antibody (2.5 μg/mL; DAKO Corp. Carpinteria, CA) for 20 minutes, rinsed with PBS, incubated in streptavidin horseradish peroxidase (2.0 μg/mL) for 20 minutes, rinsed in PBS, incubated in diaminobenzidine (DAB, 0.6 mg/mL; DAKO Corp.) for five minutes, and rinsed in water. The tissues were then counterstained with hematoxylin for four minutes, dehydrated through graded alcohols to xylene, and coverslipped.

Optical Vessel Counting: Two-person Count. Tissue sections from 18 specimens (six from each cell line variant) were analyzed. The level of α6 and β4 integrin expression was not known prior to the evaluation. Each tissue section was first observed by two investigators using a Nikon Labophot-2 microscope equipped with an SPlan 20/0.50 objective. A 488-nm filter was placed over the light source to enhance the contrast between the stained regions. Three fields of view (field diameter 0.93 mm, area 0.679 mm^2) were selected at random from each specimen and the stained regions recognized as microvessels by both investigators in consensus were counted. Vessels with and without lumens were counted. In many cases the tumor did not fill the field of view. In these cases, the tumor area was estimated by approximating the linear dimensions of a rectangle most nearly approaching the tumor area.

Optical Vessel Counting: One-person Count. The same tissue sections were observed with an Olympus BH-2 microscope equipped with an SPlan 40/0.70 objective. Six fields of view (field diameter 0.50 mm, area 0.196 mm^2) were selected at random from each specimen, and the number of stained areas recognized as vessels (with or without lumen) in each field of view was counted and recorded by a single investigator. Only areas of the tumor that filled the field of view were used for the analysis. In a few cases lack of tumor burden limited the number of fields that could be assessed. After the vessels in each field were counted, the 488-nm filter was applied and the vessels recounted. This procedure was repeated for the 18 specimens to give two repetitions of six (in most cases) fields of view for each specimen.

Computer-Assisted Methods: Vessel Numbers and Areas. Digital images of each of the filtered views observed by one investigator were then captured with a Kontron Elektronik Camera (ProgRes 3012, Germany) connected to a PC equipped with Image Manager software (version 2.2, Roche Image Analysis Systems). The digital images were exported as compressed JPEG files to a Macintosh workstation (Quadra 800), converted to TIFF files, and analyzed using NIH Image (v. 1.57, Wayne Rasband, available by anonymous FTP from zippy.nimh.nih.gov). Filtering of the incident light with a 488 nm filter during image capture produced an image in which the immunostained regions of the tumor were highly visible,

allowing for selection of those image pixels that represented the tumor vasculature.

An area of 950x725 pixels (representing an area of 0.0543 mm^2 at 400x) was selected in order to remove any artifacts from the boundaries of the image. The "Density Slice" function of NIH Image was used to select the pixels in the color range of interest, ie. those areas representing PECAM-stained vessels. "Particle Analysis", another function of the NIH Image software, was used to determine the number and the total area of the immunostained regions in a field of view. With this function, a particle was considered an area of contiguous pixels of interest whose minimum size in pixels was determined by the investigator based on the ability to screen out pixels that did not represent vessels. The computer analyzed and recorded the area of each particle and the number of particles in the region of interest. The sum of the particle areas was then reported as the total area of vascular tissue in the field of view ("Computer Area") and the number of particles was reported as the number of vessels in the field of view ("Computer Count"). This process was simplified by the writing of a "macros" to consolidate these computer functions.

Analyses were performed with minimum particle sizes of 100, 250 and 500 in order to determine whether the particle size affected the observed relationships between cell line and vascular areas. Data from the analyses were exported to spreadsheets for statistical analysis.

Measurement of Tumor Burden. Sequential images along each diaphragm section were then captured at 100x (Nikon SPlan 10/0.30) magnification using the same image-capture system mentioned above. These images were measured in order to assess whether the vascular density of the tumor correlated with the tumor height. This was accomplished using the "Measurement" tool of NIH Image, whereby the perpendicular distance from the basement membrane of the mouse diaphragm to the free surface of the tumor was measured at 250 μm intervals for each of the 18 specimens.

Measurement of Tumor Vasculature: Vascular Corrosion Casts

Preparation of Vascular Corrosion Casts. SCID mice 4-6 weeks old were injected with DU-H and DU-L cells as described above. Twenty percent of each group of mice were injected with PBS only to act as a negative control. After 28 to 36 days, the mice were anesthetized with 0.06-0.10 mL Nembutal. The abdominal cavity was surgically opened and the aorta cannulated with a 24 guage, 1.6 cm Quik-Cath intravascular over-the-needle Teflon catheter just anterior to the pelvic bifurcation. The vena cava was nicked to allow drainage of the blood, and the vascular system of the mouse perfused with heparinized PBS until the flow from the vena cava was clear. This was followed by perfusion with 2% glutaraldehyde in PBS. The glutaraldehyde step was omitted for a number of the

tumor-cell injected mice (2 DU-H, 2 DU-L, and 1 PBS-only) in order to assess the effect of tissue fixation on the quality of the vascular casts. Eight mLs of methyl-methacrylate resin (Mercox blue, Ladd Research Industries) was diluted with 2 mLs methyl methacrylate prior to adding 0.3 mL of the benzoyl peroxide. This mixture was perfused at physiological pressure (approximately 90-110 mm Hg) into the mouse vasculature until the resin appeared at the opening of the vena cava. A successful perfusion was evidenced by a blue tinge in the nose, ears, and feet of the mouse. The mouse was then placed in a bath of warm (40^{o}C) tap water for 20 minutes to allow the resin to polymerize.

The diaphragm of each mouse was removed as described above and placed in a solution of 5% KOH. The casts were gently rinsed with distilled H_2O at weekly intervals and placed in fresh portions of 5% KOH until all of the tissue had eroded from the cast, usually about four weeks. The casts were given a final rinse in distilled H_2O, then rinsed with graded ethanols (50%, 70%, 95%) and stored in absolute ethanol until they were mounted on charged slides and air dried. The casts were then photographed, first with a Pentax SF1n camera mounted on a stand 19.5 cm above the cast using a 50 mm macro lens set at 1/1, 0.15 sec shutter speed, Ektachrome 100 ASA film, and using the auto focus and auto f-stop functions of the camera. Lighting was accomplished using a lamp set at an angle oblique to the cast. Additional photographs were taken at a higher magnification using a

Nikon SMZ-2T steromicroscope with a Nikon FX-35WA camera and Nikon UFX-II exposure control with Ektachrome Elite 100 ASA film.

Confocal Laser Microscopy. Images of optical sections through the vascular cast parallel to the plane of the diaphragm were obtained using a Zeiss laser scanning confocal microscope (LSM 210) using a 400x (n.a. 0.5) magnification. The methyl-methacrylate casting resin will fluoresce at 488 nm (Hossler, 1991), allowing for the visualization of the casting material using the argon laser of the confocal microscope. The anterior surface of the cast of the diaphragm vasculature was located optically and the "z-section" function of the confocal microscope was used to acquire grayscale images at 20 μm intervals from the upper surface of the tumor vasculature through to the diaphragm vasculature as represented by the vascular corrosion cast.

Computer-Assisted Vessel Area Measurement. Quantitation of the optical sections obtained from observation of the vascular corrosion casts by confocal laser microscopy was accomplished using NIH Image. The "Threshhold" function was applied to the grayscale image of each optical section in order to select those pixels indicating the greatest intensity of fluorescence. The "Particle Analysis" function was then used to measure the areas (in pixels) of those regions in the field of view with sufficient numbers of

saturated pixels to indicate a likely tumor vessel cast. These data were exported to a spreadsheet for further analysis. A macros for the procedure was written in order to automate the analysis.

Tumor-cell Proliferation Assay

Immunohistochemistry. Frozen diaphragm tissues obtained from the same series of mice used for the immunohistochemical studies were immunostained simultaneously with the PECAM antibody (specific for endothelial cells) and MIB-1. MIB-1 is specific for the Ki-67 nuclear antigen that is expressed in the G_1, S, G_2, and M phases of cell proliferation but not in resting cells (G_0, Gerdes, 1984). Using these markers, the relative proliferation status of the the tumors arising from DU-L and DU-H cells could be compared. Frozen tissues were sectioned (3μm), fixed in cold methanol for 5 minutes, air dried, and rehydrated in PBS for five minutes. The PECAM (24 μg/mL) and MIB-1 (8 μg/mL; Immunotech, Inc., Westbrook, ME) antibodies were applied for 20 minutes in a humidified chamber, after which the slides were rinsed with PBS. The tissue was then incubated for 30 minutes with a donkey anti-rat secondary antibody coupled with Cy3 (indocarbo-cyanine, 1:800; Jackson ImmunoResearch Laboratories, Inc., West Grove, PA) and a donkey anti-mouse antibody coupled with FITC (fluorescein isothiocyanate, 1:400; Jackson ImmunoResearch Laboratories). The slides were rinsed with PBS and

coverslips applied.

Determination of Cell Proliferation Status. A laser scanning confocal microscope (Zeiss LSM 410) was used to obtain 200x images of the immunostained diaphragm tumors. Cells stained with the the MIB-1 antibody lying within a 5.07 cm^2 circular region of the image were counted. This represented an area of the tumor of _____ mm^2. Each image was sampled twice except where insufficient tumor prevented cell counting in an entire sample area.

Statistical Methods

The focus of the primary analysis was to compare the measurement parameters (average number of vessels per unit tumor area or average vessel area per unit tumor xenograft area) between the cell lines and between the imaging methods. Standard approaches to the data were inappropriate, due to the fact that observations taken from a single mouse may be presumed to be intercorrelated (personal communication, Dr. Mikel Aickin, Arizona Cancer Center, Tucson, AZ). To address this problem, the Multilevel Modeling software from the University of London was employed. The model selected one of the combinations of cell line and method of analysis as the base, and then estimated departures due to cell line and to method separately. Mice were regarded as contributing random variation within cell lines and observations were regarded

as contributing independent variation within each mouse. Consequently, the fixed parameters to be estimated were the cell line and computer-assisted measurement method. Z values for the fixed parameters were computed using the estimated departure and standard error, from which two-tailed p values could be obtained.

The variance components to be estimated were the between-mouse variance and the within-mouse variance. The within-mouse variance may be taken to represent technical variation as well as inevitable biological variation. The between-mouse variance may be taken to represent population-level biological variation. The important point about including these components is that they are necessary in order to obtain accurate estimates of the standard deviations due to either cell line and/or computer-assisted measurement method effects.

The correlation associated with the remaining parameters were analyzed by performing a t test on the mean values obtained for each specimen. The resulting t scores were used to determine two-tailed p values. The same method was used to analyze correlation between measurements taken from serial sections of immunostained tissue to assess reliability.

RESULTS

Description of Tumors

Macroscopic observation of the SCID mouse diaphragms upon removal showed variation in the quantity and distribution of the tumors growing on the inferior surface. Generally the tumors appeared as white mounds with irregular surfaces, resembling cauliflower. Some of the tumors were found isolated on the surface of the diaphragm, forming discrete, hemispherical mounds. Other tumors grew as large confluent masses, which in many cases appeared to be the result of several smaller tumors growing together. (Figure 1) The height of the tumor burden normal to the diaphragm ranged from 0.3 mm to 1.0 mm.

Vascular Density: Immunohistochemical Studies

Observation of Immunostained Tissues. Observations of the PECAM-stained SCID mouse diaphragm sections revealed a variable distribution of vessels within the tumors. Some regions of the tumor appeared to have little or no stained vessel endothelium, while other areas were well-vascularized. Vessels in some of these areas could be clearly seen to extend upward from a focal point near the diaphragm, presumably the point of entrance of the vessels into the tumor (Figure 2). In other areas, dense regions of vessel

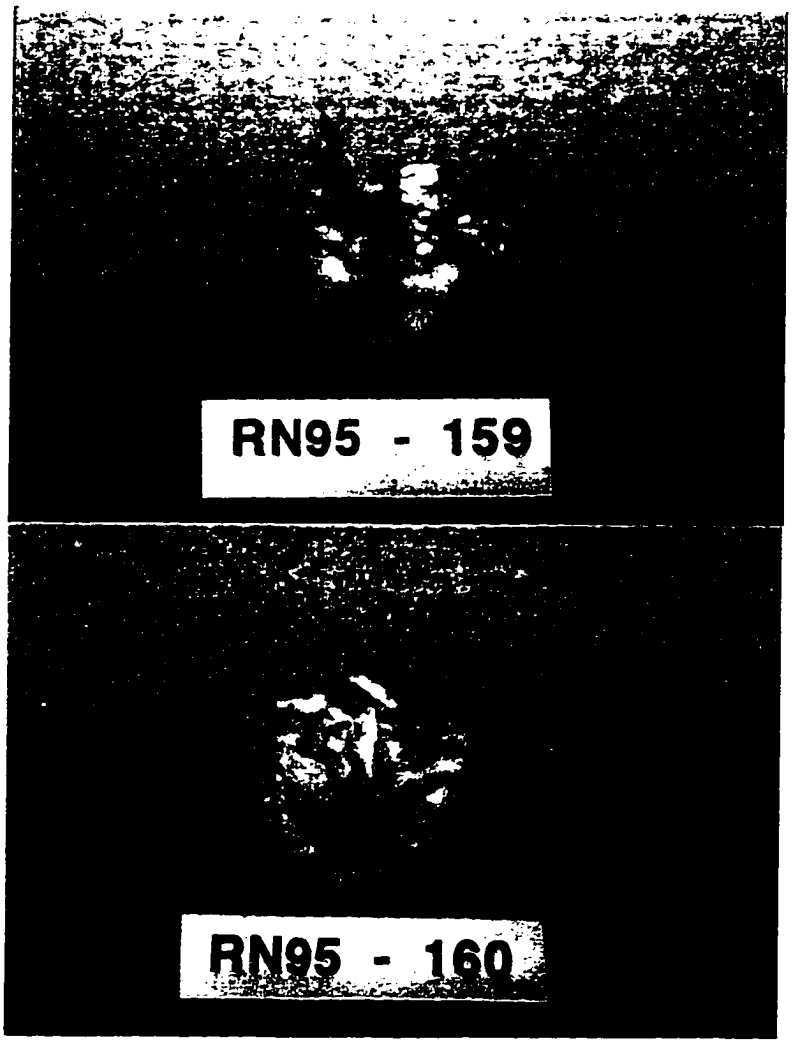

Figure 1: Excised diaphragm of SCID mouse. Upper image: Diaphragm excised from SCID mouse injected with DU-H human prostate carcinoma cells. Lower image: Diaphragm from SCID mouse injected with PBS only as a control.

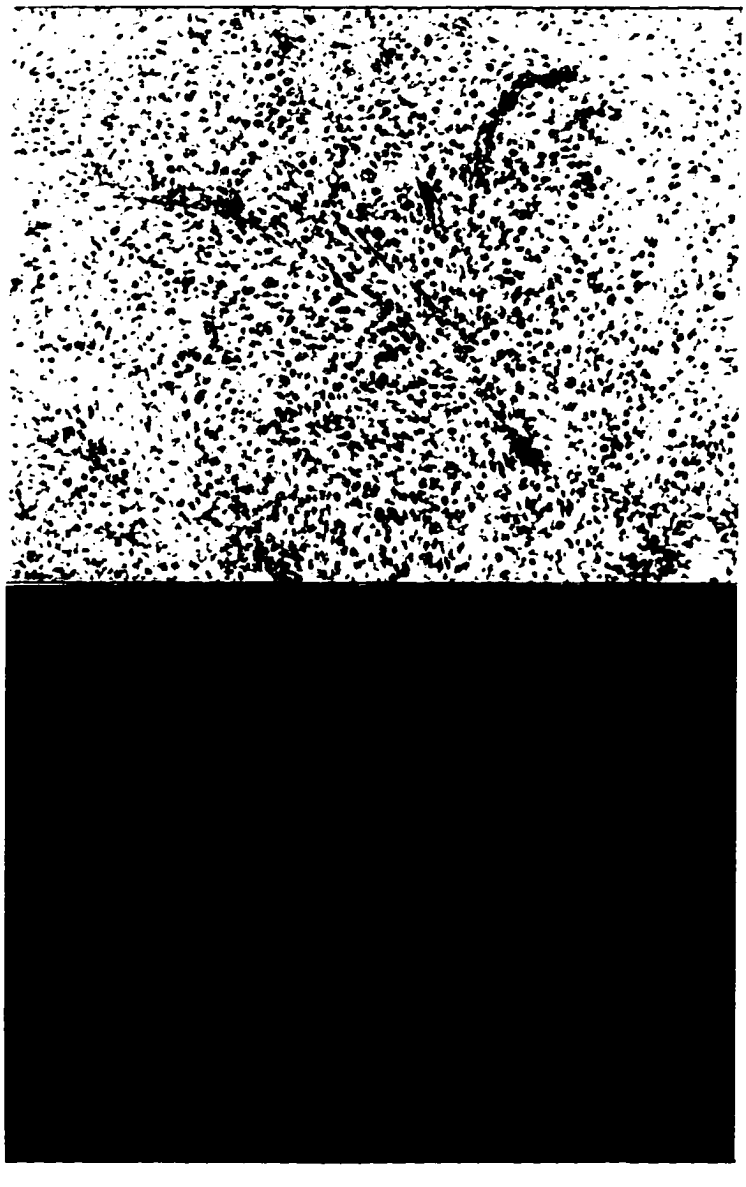

Figure 2: Conventional light micrographs of PECAM-stained SCID mouse diaphragms showing tumor xenograft vessels in branching pattern typical of isolated tumors. Upper image: Unfiltered view showing vessels stained light brown. Lower image: Same view with incident light filtered at 400 nm showing improved contrast of tumor vessels. 400x.

could be seen lying along the tumor side of the mouse diaphragm. Around many of the vessels near the point of penetration through the basement membrane, mouse fibroblasts, characterized by small, dense, uniform cell nuclei, were observed (Figure 3). Margins of the tumor did not appear well-vascularized, and necrotic regions were observed in some areas.

Optical Methods: Two-person Count. Weidner et al (1991) developed a method of tumor vessel quantitation that involved the simultaneous counting of immunostained tumor vessels in a 200x microscopic field by two observers. This method, which has been used extensively by others (Folkman, 1995) as a prognostic tool for the prediction of disease-free survival among cancer patients, was applied to the SCID mouse diaphragm tumors. The number of PECAM-immunostained vessels counted in each 200x field of view was divided by the tumor area. The mean results for each cell line are shown in Table 2. The tumors derived from cells expressing high levels of $\alpha 6$ integrin expressed primarily as $\alpha 6\beta 1$ (DU-HxV) showed the greatest number of vessels per mm^2 of tumor area, while those having high $\alpha 6$ integrin expressed primarily as $\alpha 6\beta 4$ (DU-HxB4) expression showed the least number of vessels per mm^2. Statistical analysis of the mean vascular density of the high $\alpha 6$ integrin expressers (DU-HxV and DU-HxB4) as compared to the low $\alpha 6$ integrin expressers (DU-L) showed significant

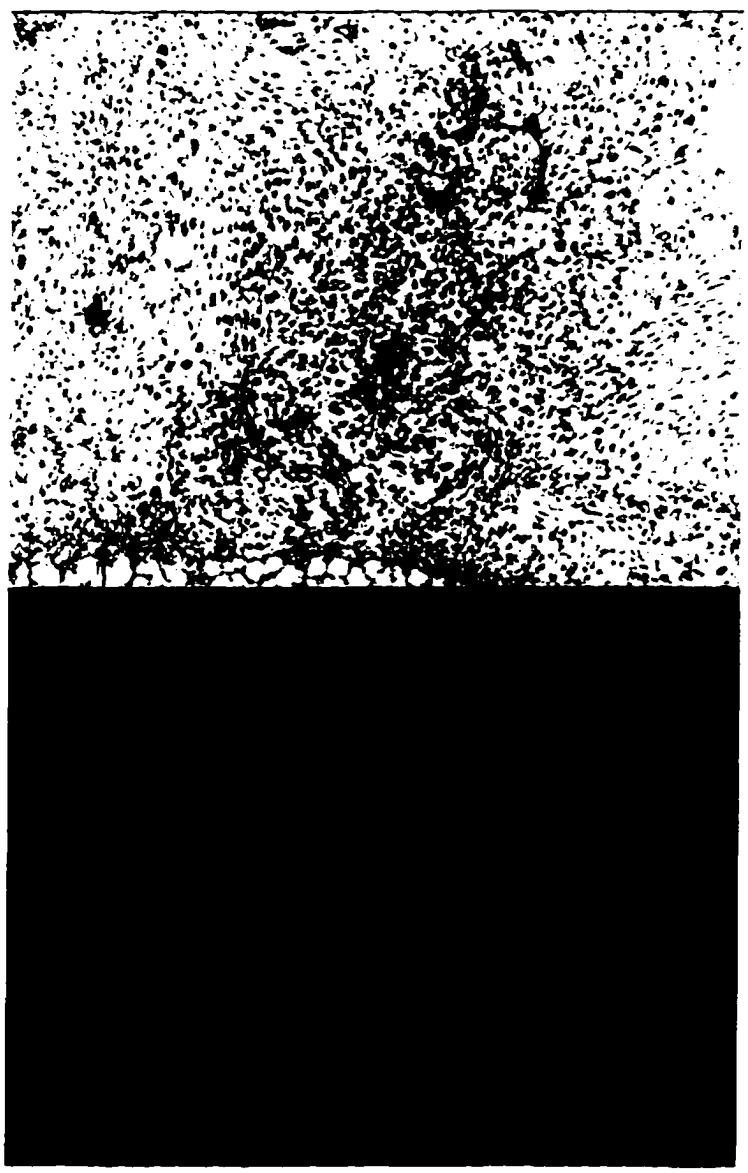

Figure 3: Conventional light micrographs of SCID mouse diaphragm tumor xenografts showing vessel plexus near the basement membrane of the mouse diaphragm. Upper image: Unfiltered view showing vessels stained light brown. Lower image: Same view with incident light filtered at 400 nm showing enhanced contrast. 400x

Table 2: Mean number of vessels per unit area of tumor xenograft using optical vessel counting methods.

Cell Line	DU-L	DU-HxV	DU-HxB4
Two person (200x field)			
Number of animal specimens	6	6	6
Total number of sample fields	18	16	18
Mean	166	288	86
(s.d., range)	(106, 75-332)	(86, 183-422)	(38, 58-157)
One person (400x field)			
Number of animal specimens	6	6	6
Total number of sample fields	32	36	36
Mean	128	95	88
(s.d., range)	(11, 117-142)	(22, 62-116)	(15, 77-114)
Correlation between methods (t-test)	p = 0.81	p = 0.22	p = 0.94

Table 3: Correlation of mean vessel counts per unit tumor xenograft area for three cell lines using optical methods of measurement.

	Cell Line Correlation		
	DU-L : DU-HxV	DU-L : DU-HwB4	DUHxV : DU-HxB4
Two-person Optical Count	Z = -3.71 (p<0.001)	Z = -2.77 (p=0.006)	Z = -0.94 (p=0.347)
One-person Optical Count	Z = -4.74 (p<0.001)	Z = -4.93 (p<0.001)	Z = -0.179 (p=0.857)

Note: Method of analysis used involved determination of the Z-score as the quotient of the difference of the means and the standard error of the mean. Differences in the mean values are considered significant if the two-tailed $p<0.05$.

differences ($p<0.001$ and $p<0.01$, respectively; Table 3). Analysis of the differences in vascular density between high α6 expressers (DU-HxV and DU-HxB4) showed no significant difference ($p>0.20$), suggesting that overexpression of β4 does not affect the vessel density in these tumors.

Optical Methods: One-person Count. The number of vessels in a 400x field of view observed with the incident light filtered at 488 nm was counted by a single observer in order to directly correlate the optical vessel counts with the computer-assisted methods. For this measurement, the DU-L tumors showed the greatest number of vessels and the DU-HwB4 tumors showed the least (Table 2). The differences between the low α6 integrin expressers (DU-L) and each of high α6 intergrin expressers (DU-HxV and DU-HxB4) were statistically significant ($p<0.001$ in both cases; Table 3). The level of β4 expression appeared to have no significant impact on the tumor vessel counts ($p>0.20$ for a correlation between DU-HxV and DU-HxB4).

The mean vessel counts for the DU-L and DU-HxB4 cell lines were similar for the two methods of counting (Table 2), but the counts obtained for the DU-HxV cell lines were significantly different. This may be the result of performing the two-person count at a magnification of 200x. At this magnification, the tumor did not fill the field of view, and the tumor area was estimated as a portion of the

field of view. This problem was most pronounced for the DU-HxV cell line, which produced the tumors with the smallest average height above the diaphragm (see below). Tumors of the other two cell lines generally filled or nearly filled the field of view. Calculation of the number of vessels per square millimeter based upon the smaller tumor areas may have introduced the error.

Computer-assisted measurements: Vessel counts. Digital analysis of images of the same 488-nm filtered 400x fields used for the one-person counts was performed using three different "particle sizes" so as to assess the impact of the selection of the particle size. Computer-assisted counting of the number of vessels in each region of interest indicated a trend similar to that seen for the one-person count (Table 4). In each case, the DU-L tumors showed the greatest number of vessels per field and the DU-HwV showed the least number. Again the vessel counts obtained for the low $\alpha 6$ integrin expressers were significantly higher than that of either of the high $\alpha 6$ integrin expressers ($p<0.001$ in both cases for all three particle sizes; Table 5). Differences between the vessel counts for the two high $\alpha 6$ expressers were not significantly different for any of the particle sizes used ($p=0.857$), again suggesting that $\beta 4$ integrin expression does not affect tumor vessel density.

The computer-assisted vessel counts using a particle

Table 4: Mean number of vessels per unit tumor xenograft area using computer-assisted vess counting methods.

Cell Line	DU-L	DU-HxV	DU-HxB4
Number of animal specimens	6	6	6
Total number of sample fields	32	36	36
Computer-assisted vessel count (vessels per sq mm)	Mean (s.d., range)	Mean (s.d., range)	Mean (s.d., range)
Particle size 100	525 (301, 273-1105)	224 (97, 132-393)	261 (110, 120-396)
Particle size 250	219 (84, 110-328)	121 (90, 46-298)	142 (55, 68-203)
Particle size 500	180 (45, 129-236)	99 (67, 49-230)	101 (56, 34-178)
Correlation between methods (Z-test)			
PS 100 : PS 250	$p < 0.001$	$p < 0.001$	$p < 0.001$
PS 100 : PS 500	$p < 0.001$	$p < 0.001$	$p < 0.001$
PS 250 : PS 500	$p = 0.254$	$p = 0.254$	$p = 0.254$

Table 5: Correlation of mean vessel counts per unit tumor xenograft area for three cell lines using computer-assisted methods of measurement.

	Cell Line Correlation		
	DU-L : DU-HxV	DU-L : DU-HxB4	DU-HxV : DU-HxB4
Computer-assisted Count			
100 Particle Size	Z=-4.74 (p<0.001)	Z = -4.93 (p<0.001)	Z = -0.179 (p=0.857)
250 Particle Size	Z = -4.74 (p<0.001)	Z = -4.93 (p<0.001)	Z = -0.179 (p=0.857)
500 Particle Size	Z = -4.74 (p<0.001)	Z = -4.93 (p<0.001)	Z = -0.179 (p=0.857)

Note: Method of analysis used involved determination of the Z-score as the quotient of the difference of the means and the standard error of the mean. Differences in the mean values are considered significant if the two-tailed $p<0.05$.

size of 250 and 500 did not correlate for any of the cell lines ($p=0.254$) and both were significantly different from the computer counts made using a particle size of 100 ($p<0.001$ in both cases). The one-person vessel counts differed significantly from the 250 and the 500 particle-size computer count ($p<0.001$) but not the 100 particle-size computer count ($p=0.17$).

Computer-assisted measurements: Vessel area. Digital analysis of images of the same 488-nm filtered 400x fields used for the one-person and computer counts was performed using three different "particle sizes" so as to assess the impact of the selection of the particle size. It can be seen from Table 6 that the trends for the mean values of the total vessel areas represented as the area in micrometers representing vessel endothelium per millimeter of tumor are the same for all three particle sizes. In all cases the DU-L tumors showed the greatest total vessel area while the DU-HwV tumors showed the least. Results in Table 7 indicate that the mean total vessel area for the low $\alpha 6$ integrin expressers was significantly higher than the mean total vessel area for the tumors produced by DU-HxV cells ($p<0.001$), but not for the the tumors produced by DU-HxB4 cells ($p=0.056$). Tumors of high $\beta 4$ integrin expressers did not show significantly greater vessel area than those of low $\beta 4$ integrin expressers ($p=0.347$) for all three particle sizes.

Table 6: Mean vessel area per unit tumor xenograft area using computer-assisted area measurement methods.

Method	Cell Line Mean Values (sq mm vessel per sq mm tumor) DU-L	DU-HxV	DU-HxB4
Number of animal specimens	6	6	6
Total number of sample sites	32	36	36
Particle size 100			
Mean	0.0568	0.0158	0.0242
(s.d., range)	(0.0393, 0.0231-0.1297)	(0.0149, 0.0027-0.0387)	(0.0238,0 .0049-0.0634)
Particle size 250			
Mean	0.0023	0.00096	0.0015
(s.d., range)	(0.0008, 0.0007-0.0030)	(0.0011, 0.0001-0.0030)	(0.0013, 0.0004-0.0036)
Particle size 500			
Mean	0.0350	0.0132	0.0201
(s.d., range)	(0.0137, 0.0208-0.0553)	(0.0128, 0.0020-0.0354)	(0.0213, 0.0032-0.0544)
Correlation between methods (Z-test)			
PS 100 : PS 250	$p < 0.001$	$p < 0.001$	$p < 0.001$
PS 100 : PS 500	$p = 0.089$	$p = 0.089$	$p = 0.089$
PS 250 : PS 500	$p < 0.001$	$p < 0.001$	$p < 0.001$

Analysis showed that the selection of particle size resulted in significant differences in the vessel areas for the 250 particle size for all three cell lines when compared with either of the other two particle sizes used ($p<0.001$ in all cases) but that the observed mean values for the 100 particle size and the 500 particle size were not significantly different ($p=0.089$) for any of the cell lines (Table 6).

Evaluation of Immunohistochemical Methods of Measuring Tumor Xenograft Vessel Density. One-person optical vessel counts were made both with and without the 488 nm filter to ensure the reliability of the counting method. Correlation was high ($p=0.90$), suggesting that the use of the filtered images both for the optical vessel counting and for the computer-assisted methods was reliable. This enabled the computer selection of those regions of the tumor representing vascular tissue.

Consecutive serial sections of one of the low $\alpha 6$-expresser diaphragm tumors (DU-L) were evaluated using each of the methods except the two-person vessel count (Table 8). Analysis of the results using a t-test for each method revealed correlations between the values for the methods used ($p>0.50$ for all methods), although the correlations were not high. The most reliable method appeared to be the one-person count ($p=0.88$).

A measure of the reliability of the mouse model was found in the determination of the variance within mice using

Table 7: Correlation of mean tumor vessel areas per unit tumor xenograft area for three cell lines using computer-assisted measurement methods.

	Cell Line Correlation		
	DU-L : DU-HxV	DU-L : DU-HxB4	DU-HxV : DU-HxB4
Computer Area 100	Z = -3.71 (p<0.001)	Z = -2.77 (p=0.056)	Z = -0.94 (p=0.347)
Computer Area 250	Z = -3.71 (p<0.001)	Z = -2.77 (p=0.056)	Z = -0.94 (p=0.347)
Computer Area 500	Z = -3.71 (p<0.001)	Z = -2.77 (p=0.056)	Z = -0.94 (p=0.347)

Note: Method of analysis used involved determination of the Z-score as the quotient of the difference of the means and the standard error of the mean. Differences in the mean values are considered significant if the two-tailed $p<0.05$.

Table 8: Study of reliability of selected methods of tumor xenograft vessel quantitation.

Method	Mean (s.d.) Section A	Section B	t	p
One-person vessel count (vessels per sq mm)	138 (68)	151 (67)	0.16	0.88
Number of fields	12	6		
Computer-assisted vessel count (vessels per sq mm)				
Particle size 100	133 (47)	99 (39)	0.43	0.67
Particle size 250	91 (35)	64 (30)	0.53	0.61
Particle size 500	63 (24)	42 (17)	0.59	0.57
Number of fields	6	6		
Computer-assisted area measure (sq um vessel per sq mm tumor)				
Particle size 100	0.0362(0.0132)	0.0288(0.0110)	0.34	0.74
Particle size 250	0.0030(0.0011)	0.0024(0.0009)	0.34	0.74
Particle size 500	0.0313(0.0128)	0.0251(0.0111)	0.35	0.74
Number of fields	6	6		

Note: Sections A and B are serial sections of a SCID mouse diaphragm bearing DU-145L tumor

the Z test. This was found to be high (77.1, or 89% of the total variance, for the vessel counting methods and 103.8, or 54% of the total variance, for the vessel area measurements), suggesting considerable variation in the distribution of vessels within the tumors of each mouse.

The variance between mice obtained from the Z test for the computer area methods was high (45% of the total variance, data not shown), suggesting that differences in the mean values may be significantly affected by methodological factors. Between-mouse variance for the vessel counting methods was low (11.0%), suggesting a more generally reliable method than the computer-assisted area measurement.

Computer-Assisted Measurement: Tumor Burden. The dimensions of the tumor burden as a function of α6 and β4 integrin expression was also assessed by measuring the height of the tumor from the basement membrane of the murine diaphragm to the outer (peritoneal) surface of the tumor using the "Measurement" function of NIH Image. The mean values for each cell line (Table 9) show that the DU-L tumors have the greatest height (and thus, presumably, the greatest volume) while the DU-HwV tumors have the least height. Analysis of the mean values using a t-test indicated no significant differences in the tumor heights produced by the three cell lines ($p>0.05$ in all cases; Table 10). The number of sites measured was taken to be a measure of the extent of tumor spread across the diaphragm, and in this case the low α6

Table 9: Measurement of tumor xenograft height using computer-assisted methods.

	Cell Line Mean Values (std.dev.)		
	DU-L	DU-HxV	DU-HxB4
Number of animal specimens	6	6	6
Tumor height (um)	726 (500)	430 (72.5)	633 (207)
Number of measurements per specimen	21.7 (9.3)	36.7 (12.2)	39.8 (18.7)

Table 10: Correlation between cell lines for tumor xenograft height using computer-assisted methods.

	Cell Line Correlation		
	DU-L : DU-HxV	DU-L : DU-HxB4	DU-HxV : DU-HxB4
Tumor Depth	t = 0.69 (p=0.506)	t = 0.19 (p=0.853)	t = 0.57 (p=0.581)
Number of Measures	t = 0.76 (p=0.465)	t = 0.84 (p=0.421)	t = 0.12 (p=0.907)

Note: Correlation evaluated using two-tailed t-test.

integrin expresser tumors seemed to cover the least amount of diaphragm surface (Table 9), although the differences were not significant ($p>0.05$ for all cases; Table 10).

Vascular Density: Vascular Cast Studies

Observations of vascular corrosion casts. Observation of the vascular corrosion casts showed a similar pattern to the vascular beds of the tumors evident on the surface of the diaphragm. The vascular bed of the normal mouse diaphragm consisted of small vessels that lay roughly parallel to each other and radiated from the center of the diaphragm, near the locus of penetration of the vena cava, to the margins, resulting in a striated appearance. (Figure 4) When observed in isolation these vessels exhibited a wavy configuration with no branching. These smaller vessels appeared to branch from larger vessels that in turn originated from a large vessel that ringed the inner avascular region of the diaphragm.

In the smaller isolated tumors, the vasculature consisted of several vessels arising more or less perpendicular to the plane of the diaphragm. It appeared that these vessels originated from a single mouse diaphragm vessel, grew upward from the diaphragm vasculature into the tumor, and formed closed loops near the margins of the tumor, although the origin of the tumor vessels growing normal to

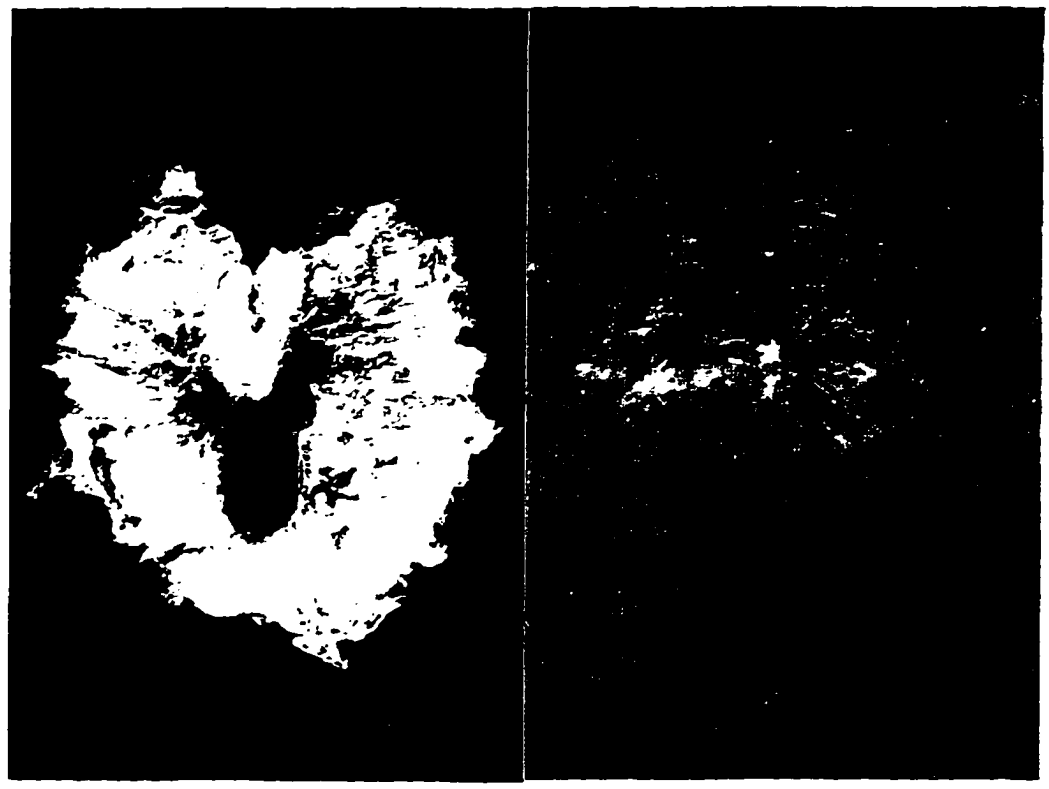

Figure 4: Vascular corrosion cast of SCID mouse diaphragm. Left: Typical cast from SCID mouse injected with DU-145L human prostate carcinoma cells (2x). Right: View of vascular cast showing parallel arrangement of vessels in the diaphragm and tumor vessels growing out of the the diaphragm vasculature. 15x

the plane of the diaphragm vasculature was difficult to view.

In the smaller tumors there was evidence of lateral branching of the vessels to form networks. The tumor vessels had markedly larger diameters than the vessels of the untreated diaphragm. Vessels sometimes appeared to be distended near the periphery of the tumor, perhaps reflecting distortion of the vessel due to high pressures exerted by the casting material as it entered the vessel. The interior regions of these small tumors appeared to lack vessels, giving the effect of a hollow vascular net.

In the areas in which the tumor coverage of the diaphragm was broad the arrangment of the vessels in the tumor appeared to be much more complex. The casting material in these tumors formed a very fine network reflecting extensive branching and rebranching of the vessels. In none of the tumor vasculature did there appear to be any regular pattern of branching, although often near the outer margins of the tumor vessels appeared to form ring-like structures. Numerous vessel buds could also be seen in these areas.

In many regions where tumors had not developed there appeared to be a low dense plexus of vessels barely rising above the diaphragm vasculature. These vessels appeared relatively large compared to other tumor vessels and showed numerous buds projecting above the plane of the diaphragm vasculature. These plexuses were especially apparent around many of the isolated tumors, leaving what appeared as a crater near the avascular center of the tumor (Figure 5).

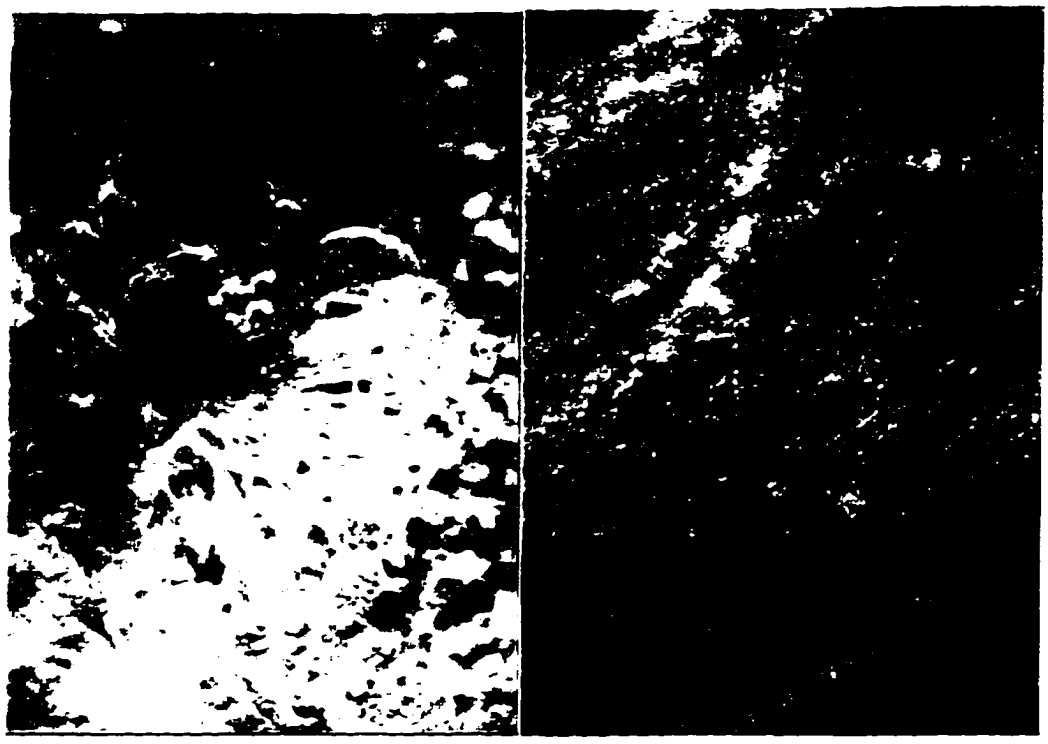

Figure 5: Vascular corrosion casts of tumor xenografts. Left: View showing dense mat of vessels overlying diaphragm vasculature with larger branched vessels arising normal to the plane of the diaphragm. Right: Similar view showing parallel arrangement of underlying diaphragm vessels overlaid with dense plexus of tumor vessels. Hollowed circular areas may represent tumor necrosis. (15x)

Casts obtained from mice that had not been perfused with glutaraldehyde prior to perfusion with the casting material showed evidence of distortion of the vessels. In particular there was much more evidence of vessel rupture and the formation of small rounded balls of casting material in various regions. If the perfusion pressures were sufficient to cause rupture of the vessels, it is likely that other vessels were distorted even though they did not break open.

Examination of the digital images obtained by confocal laser microscopy appeared to confirm some of the observations noted above. Sequential images taken at regular intervals along the axis normal to the plane of the mouse diaphragm tended to show open areas in the interior of isolated tumors and a region of high vascular density near the surface of the diaphragm, which may correspond to the plexuses noted above. Three-dimensional reconstructions generated from false-colored optical sections also show the lack of vessels in the interior of the tumor. (Figure 6)

Measurement of Vascular Density from Vascular Corrosion Casts. Difficulties in determining the optimal conditions for confocal laser microscopy and variation in the integrity of the vascular casts prevented a thorough evaluation of the tumor vasculature using this method. However, some preliminary results were obtained that indicate quantitative differences in the vasculature of tumors produced by the DU-145 variants. Table 11 shows the mean values for the area of

Figure 6: Computer enhanced three-dimensional resconstruction of microvessel architecture in tumor xenografts. Blue color represents the plane closest to the diaphragm and red represents the plane farthest from the diaphragm. Note the apparent absence of vessels in the tumor interior and the irregular vessel size. 200x.

Table 11: Results of comparison of mean vessel area fraction and mean tumor vasculature height using vascular corrosion casts and confocal laser microscopy.

	DU-L	DU-H		
Number of Specimens	2	2		
Number of sample sites	8	11		
Vessel area (sq mm vessel per sq mm tumor)				
Mean	0.0253	0.0199	t=0.24	p=0.83
(s.d.)	0.0264	0.0187		
Height of tumor vasculature (um)				
Mean	1235	885	t=1.22	p=0.35
(s.d.)	375	18		

the vasculature per unit tumor area, shows that the differences seen in the tumor vasculature from the low α6 and high α6 integrin expresser tumors were not significantly different. The same was true of the mean tumor vasculature height, as determined by counting the number of confocal optical sections and multiplying by the interval between sections. These results are very tentative due to difficulties with optimization of the meaasurement techniques and the small sample size, but serve to suggest a possible mechanism by which the density of the tumor vasculature could be quantified.

Tumor cell proliferation studies

Observation of PECAM/MIB-1 Immunostained Tissues. Simultaneous double immunostaining of frozen diaphragms with the anti-mouse PECAM antibody and the MIB-1 anti-Ki-67 antibody from the same series used for the vascular quantitation noted above allowed for the evaluation of the effect of α6 integrin expression on the proliferative rate of the tumor cells. (Figure 7) Immunostaining presented a variable intensity, perhaps due to quenching of the fluorescent dye while examining each section. Vessel endothelium was clearly marked PECAM antibody. Areas around vascular endothelium appeared to have a lower density of proliferating cells.

Measurements of Status of Proliferation. Results (Table 12) show that DU-L tumor cells have a significantly higher number of proliferating cells than the DU-HxV tumor cells ($p=0.047$; Table 13), but not the DU-HxB4 tumor cells ($p=0.075$). The numbers of proliferating cells in tumors produced by the DU-HxV and DU-HxB4 lines cells show no significant difference ($p=0.148$).

Figure 7: Confocal laser micrograph of SCID mouse diaphragm tumor double immunostained with PECAM antibody (red) highlighting mouse endothelium in the tumor microvessels and MIB-1 highlighting the proliferating human prostate tumor cells (green). 200x

Table 12: Summary of results of DU-145 tumor cell proliferation study.

Cell Line	DU- L		DU- HxV		DU- HxB4	
Specimen	1	2	1	2	1	2
Number of sample sites	6	36	27	20	34	36
Mean number of proliferating cells per field (std.dev.)	22.3 (8.0)	18.4 (7.9)	11.2 (6.3)	8.6 (7.1)	13.9 (5.8)	12.6 (4.1)
Cell line mean (std. dev.)		18.9 (7.9)		10.1 (6.1)		13.3 (5.0)

Table 13: Correlation of tumor cell proliferation rates between cell lines.

	Cell Line		
	DU-L: DU-HxV	DU-L:DU-HxB4	DU-HxV:DU-HxB4
Tumor Cell Proliferation	t = 4.46 (p=0.047)	t = 3.45 (p=0.075)	t = 2.30 (p=0.148)

Note: Correlation evaluated using two-tailed t-test.

DISCUSSION

α6β1 and α6β4 Integrin Expression and Tumor Vessel Density

In this study five distinct methods of evaluating the microvessel density in human prostate tumor xenografts in the SCID mouse diaphragm were used to assess the effect of α6β1 and α6β4 integrin expression on the development of tumor vasculature. Three of the methods (one-person count, computer count, and computer area) showed that the density of microvessels is 1.2-2.7 times greater in those tumors resulting from the intraperitoneal injection of DU-145L cells (Figure 8 and Figure 9), which exhibit weak expression of the α6 integrin subunit, primarily as α6β4 (Rabinovitz, 1995). The effect of the higher α6 integrin expression on tumor microvessel density was not influenced by β4 integrin expression, which is dominant to β1 integrin in binding to α6 integrin (Cress, 1995).

These methods did not correlate well with each other. This result leaves in doubt whether any of these methods provides an accurate measure of the tumor microvessel density. Brawer (1994) found a high correlation between microvessel quantitation by optical counting and by computer-assisted vessel area measurement, but this was not borne out

Figure 8: Number of vessels per square mm in SCID mouse diaphragm tumor generated by DU-145 human prostate carcinoma cell line variants.

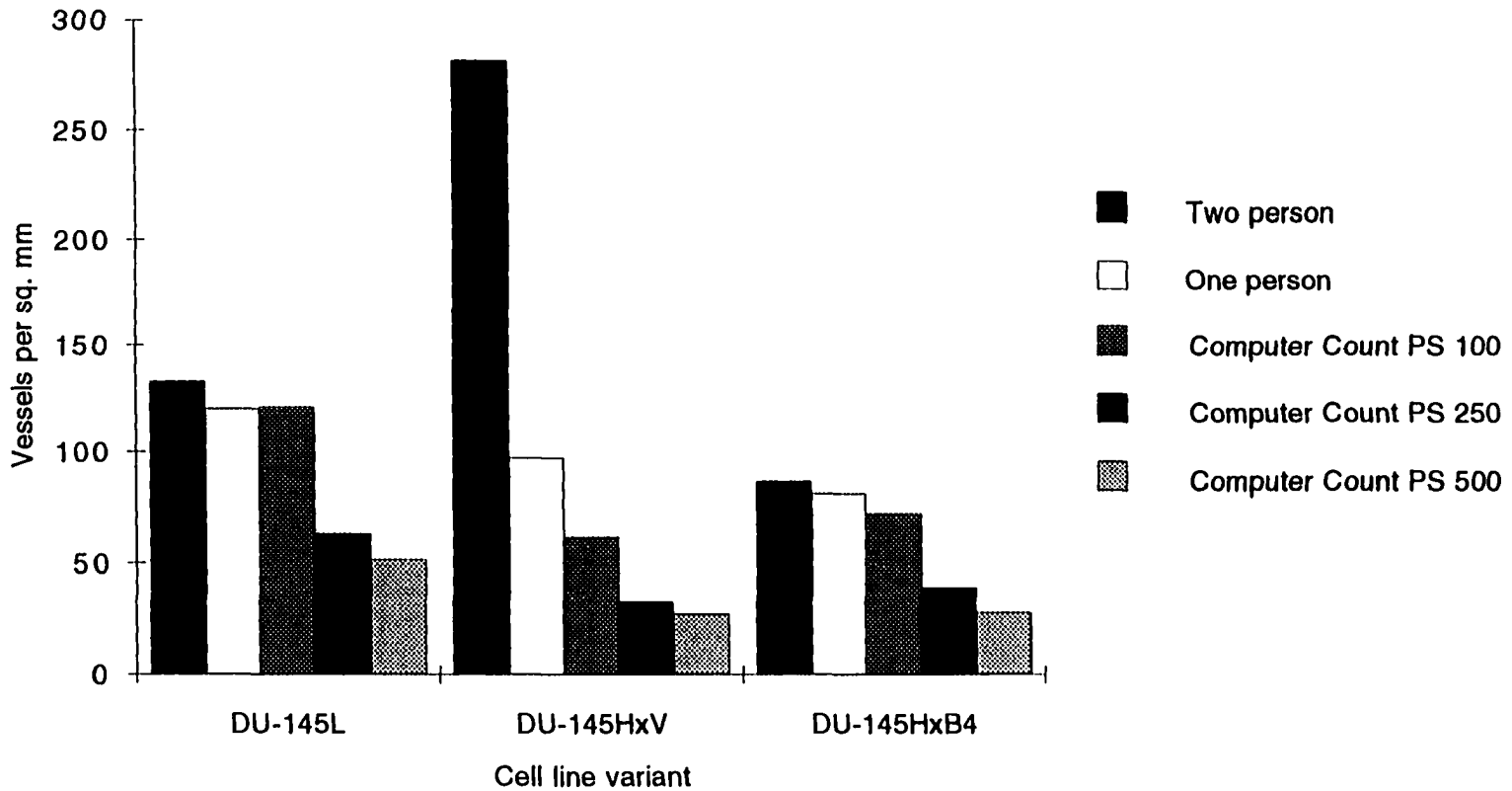

Figure 9: Results of tumor xenograft vessel area measurements using computer-assisted methods.

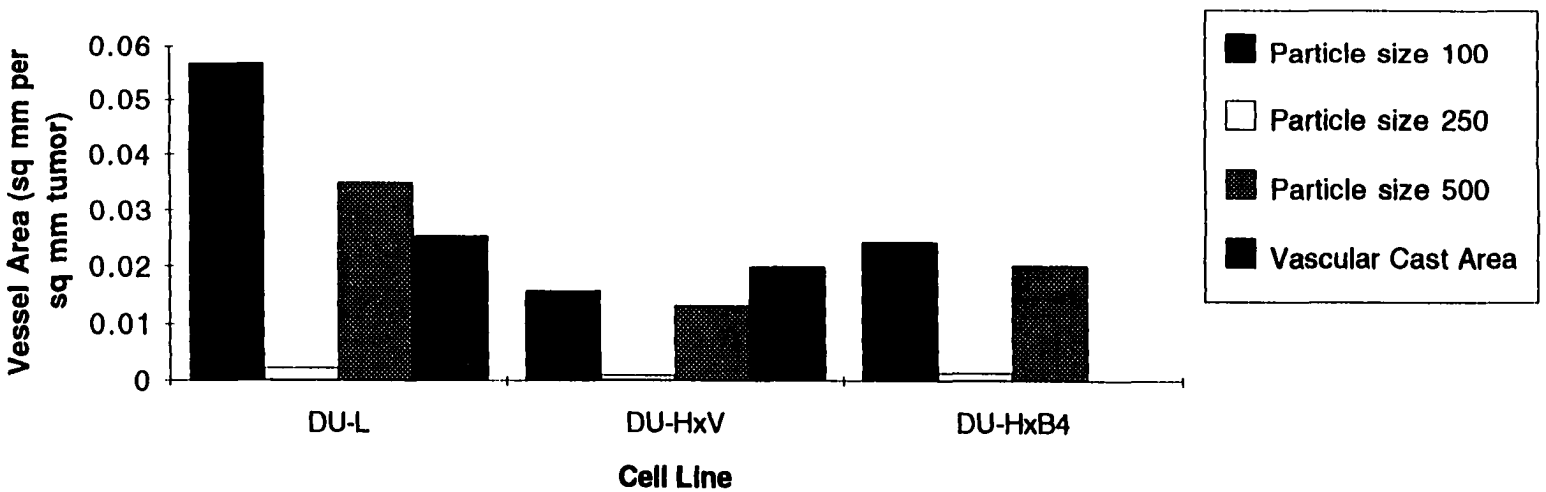

in the current study. In spite of the variability in the results obtained by the different methods, all of these methods showed a consistently significant effect of α6 integrin expression onthe tumor vessel density. Thus, while the methods did not correlate well with each other, the trends in the results were remarkably similar and suggest real differences in the effect of the α6 integrin subunit on the vascularization of the tumors.

Comparison of measurements obtained from serial tumor/diaphragm sections show that these three methods produce consistent results, with the one-person vessel count showing the greatest reliability ($p=0.88$). It is interesting to note that the computer count and the computer area determinations for the serial sections also showed correlation between the sample determinations (Table 8). As both of the sections analyzed were on the same slide and were subjected to the same immunostaining procedures, the correlation may indicate that the variability seen between different tumors generated by the same cell line may be due not to the methods of quantitation but to the effectiveness of the staining procedures, as noted by Weidner (1995).

Variability in the vessel counts obtained by computer-assisted methods using different particle sizes were expected. The analysis using a particle size of 100 correlated best with the optical counts. Use of the smaller particle size tends to include more of the smaller vessels and single endothelial cells, as recommended by many

investigators (Bosari, 1992; Weidner, 1993; Hollingsworth, 1995; Folkman, 1995).

Analysis of the variability of the results obtained by the vessel-counting methods as a whole indicates that the variability between measurements taken from a single tumor was high, as was expected given the heterogeneity of the tumor vasculature. The low value for the between-mouse variability suggests consistency in the methodology. Methods employed to measure vessel area also showed high within-mouse variability, but the between-mouse variability was also high, suggesting that these methods were less reliable. Kohlberger (1996) compared computer-assisted image analysis with established counting methods using Factor VIII-related antigen to identify the tumor vessels and found that the area measurement was not a reliable indicator of prognosis. It was suggested in that study that the orientation of the vessel during sectioning can lead to wide variability in the area presented by each vessel, and hence an unreliable measure of tumor vasculature. This may be of particular significance in the assessment of vascularity in a directional tumor such as found in the SCID mouse model. The results of this study tend to confirm this.

Two-person optical vessel counting gave different results, with the tumors produced by the DU-145HxV showing the greatest vessel density. This assay was performed at 200x, the magnification suggested by Weidner (1991), whereas the other vessel counts were performed at 400x. At 200x, the

tumors generated by the DU-L and DU-HxB4 variants were large enough that regions could be found that filled the field of view, allowing for the standardization of the tumor area assayed. Variation in vessel density that normally occurs in tumors (Konerding, 1992; Weidner, 1995) tended to be averaged over the entire field of view. However, in the tumors generated by the DU-HxV variants the tumors were small and it was difficult to precisely determine the area of the tumor, thus perhaps introducing error into the determination of the vessel count-to-tumor area ratio due to underestimation of the tumor area. Repeat analysis using the two-person counting method at 400x magnification may yield results more consistent with the above findings.

Analysis of confocal laser micrographs of vascular corrosion casts also did not support the finding of differences in tumor vessel density. However, analyses were limited in scope, in part due to difficulties in determining optimal microscope parameters (pinhole, offset, and gain) necessary for obtaining reliable data. Also, the only method of tumor vessel quantitation used was vessel area per unit area of field of view. The vessel area per unit tumor area determination was also shown to be the least effective of the approaches using the PECAM-immunostained tissues and conventional microscopy. Reanalysis of digital images of the optical sections obtained by the confocal microscope by vessel counting under optimized conditions may yield results that are more consistent with those mentioned above.

Tumor Growth

Tumor size. The apparent macroscopic differences in the tumors produced by the DU-H and DU-L cell lines were not supported by the quantitative measurement of the tumor height by two methods: measurement using digital images of PECAM-immunostained tumors and counting the number of optical sections of vascular corrosion casts using the confocal laser microscope. The low α6 integrin expresser tumors appeared to be of greater height and more limited spread on the diaphragm in the PECAM-stained tumors and of greater height from the vascular corrosion casts, correlating with previous impressions of greater tumor burden among tumors produced by DU-L cells. However, these differences were not statistically significant. There was, in fact, a weak correlation between the tumor heights for the three cell lines. This may have resulted from the four-fold increase of DU-H tumor cells injected into each mouse compared to the number of DU-L cells.

The apparent but statistically insignificant increase in the spread of the DU-H tumors on the diaphragm may be the result of more of the injected tumor cells seeding onto the diaphragm, resulting in an increase in number of tumor initiation sites. The development of the tumor burden may also be dependent on other factors such as cell loss from the tumor due to poor adhesion and/or programmed cell death (apoptosis).

Tumor cell proliferation

Differences in the proliferation status were significant between the DU-L and DU-H cell lines. Mean values for proliferation would suggest that the DU-145L tumor cells proliferate at a higher rate, but variability in the data is high, with coefficients of variability ranging from 0.38 to 0.60, and the probability that the differences were due to factors other than chance was near the threshold ($p=0.046$). This portion of the study is limited by the small sample size, and variability in immunostaining and biases involved in selecting proliferating cells from the images may have contributed to the uncertainty of the results.

The difference in proliferation status has been observed qualitatively in a previous study. Rabinovitz (1995) found an increased proliferative rate for the low $\alpha 6$ integrin expressers *in vivo*. This the basis for the elevation of the number of DU-H cells injected in the SCID mice relative to the number of DU-L cells. Other investigators have found no correlation between tumor cell proliferation and tumor vascularity (Weidner, 1992; Fox, 1993). Further study is suggested to accurately assess the effect of $\alpha 6\beta 1$ and $\alpha 6\beta 4$ integrin expression on cell proliferation rate.

Conclusions

The results of this study suggest that the expression of the α6 integrin subunit in human prostate tumors negatively correlates with intratumor microvessel density, but that association of the β1 and β4 integrin subunits with the α6 integrin subunit does not influence the vascular density of the tumors. Whether this is a causal relationship is unknown. Studies of the signaling mechanisms leading to angiogenesis of tumors suggest a very complex view of the nature of the interaction of the tumor cell with the host vascular system (Weidner, 1995; Fox, 1996; Senger, 1996), and offer fertile ground for further studies.

This study also suggests that there are no significant differences in the size of the tumors produced by cells presenting different levels of either α6 or β4 integrin expression. Increased intratumoral microvessel density appears to be correlated with increased tumor cell proliferation. However, the significance of this association remains unclear due to the limited nature of this portion of the study.

Finally, this study suggests that computer-assisted microvessel counts can reliably approximate vessel counts obtained by human observers and avoid biases introduced by the introduction of subjective criteria for the identification of relevant indicators of tumor vasculature.

Further, the computer-assisted vessel counts may offer improved reliability over area determinations. Filtering of the incident light and automated algorithms allow for computer selection of immunostained regions without extensive image manipulation, thus reducing analysis time and the effects of observer bias.

References

Abe, Y., K. Sugisaki, and A.M. Dannenberg, Jr. 1996. Rabbit vascular endothelial adhesion molecules: ELAM-1 is most elevated in acute inflammation, whereas VCAM-1 and ICAM-1 predominate in chronic inflammation. J. Leukoc. Biol. 60:692-703.

Alberts, B., D. Bray, J. Lewis, K. Roberts, and J.D. Watson. 1994. Molecular Biology of the Cell. Garland Publishing, Inc. New York.

Bosari, S., A.K.C. Lee, R.A. DeLellis, B.D. Wiley, G.J. Heatley, and M.L. Silverman. 1992. Microvessel Quantitation and Prognosis in Invasive Breast Carcinoma. Hum Pathol. 23:755-61.

Brawer, M.K., R.E. Deering, M. Brown, S.D. Preston, and S.A. Bigler. 1994. Predictors of Pathologic Stage in Prostate Carcinoma: The Role of Neovascularity. Cancer 73:678-87.

Brawer, M.K. 1996. Quantitative Microvessel Density: A Staging and Prognostic Marker for Human Prostatic Carcinoma. Cancer 78:345-9.

Buck, C.A. 1995. Adhesion Mechanisms controlling Cell-Cell and Cell-Matrix Interactions During the Metastatic Process. p. 172-205. In J. Mendelsohn, P.M. Howley, M.A. Israel, and L.A. Liotta (eds.), Molecular Basis of Cancer. W.B. Saunders Co., Philadelphia.

Chammas, R., and R. Brentanni. 1991. Integrins and Metastases: An Overview. Tumor Biol. 12:309-320.

Cox, D., T. Aoki, J. Seki, Y. Motoyama, and K. Yoshida. 1994. The Pharmacology of the Integrins. Med. Res. Rev. 14:195-228.

Cress, A.E., I. Rabinovitz, W. Zhu, and R.B. Nagle. 1995. The $\alpha 6\beta 1$ and $\alpha 6\beta 4$ integrins in human prostate cancer progression. Cancer Met. Rev. 14:219-28.

Fidler, I.J., and L.M. Ellis. 1994. The Implications of Angiogenesis for the Biology and Therapy of Cancer Metastasis. Cell 79:185-88.

Folkman, J. and C. Haudenschild. 1980. Angiogenesis *in vitro*. Nature 288:551-558.

Folkman, J., and M. Klagsbrun. 1987. Angiogenic Factors. Science 235:442-447.

Folkman, J. 1995. Tumor Angiogenesis p. 206-232. In J. Mendelsohn, P.M. Howley, M.A. Israel, and L.A. Liotta (eds.), Molecular Basis of Cancer. W.B. Saunders Co., Philadelphia.

Fontanini, G., S. Vignati, F. Pacini, L. Pollina, and F. Basolo. 1996. Microvessel count: an indicator of poor outcome in medullary thyroid carcinoma but not in other types of carcinoma. Mod. Pathol. 9:636-41.

Fox, S.B., K.C. Gatter, and A.L. Harris. 1996. Tumour Angiogenesis. J. Pathol. 179:232-7.

Gerdes, J., H. Lemke, H. Balsch, H.H. Wacker, U. Schwab, H. Stein. 1984. Cell cycle analysis of a cell-proliferation associated human nuclear antigen defined by the monoclonal antibody Ki-67. J. Immunol. 133:1710-15.

Giatromanolaki, A., M. Koukourakis, K. O'Byrne, S. Fox, R. Whitehouse, D.C. Talbot, A.L. Harris, and K.C. Gatter. 1996. Prognostic value of angiogenesis in operable non-small cell lung cancer. J. Pathol. 179:80-8.

Hollingsworth, H.C., E.C. Kohn, S.M. Steinberg, M.L. Rothenberg, and M.J. Merino. 1995. Tumor Angiogenesis in Advanced Stage Ovarian Carcinoma. Amer. J. Pathol. 147:33-41.

Hossler, F.E., J.E. Douglas, A. Verghese, and L. Neal. 1991. Microvascular Architecture of the Elastase Emphysemic Hamster Lung. J. Electron Microsc. Technique 19:406-18.

Iwahana, M., Y. Nakayama, N.G. Tanaka, M. Goryo, and K. Okada. 1996. Quantification of tumour-induced angiogenesis by image analysis. Intl. J. Exp. Pathol. 77:109-14.

Juliano, R.L., and J.A. Varner. 1993. Adhesion molecules in cancer: the role of integrins. Curr. Opin. Cell Biol. 5:812-818.

Kibbey, M.C., D.S. Grant, and H.K. Kleinman. 1992. Role of the SIKVAV Site of Laminin in Promotion of Angiogenesis and Tumor Growth: An In Vivo Matrigel Model. J. Natl. Cancer Inst. 84:1633-38.

Kohlberger, P.D., A. Obermair, G. Sluitz, H. Heinzl, H. Koelbl, G. Breitenecker, G. Gitsch, and C. Kainz. 1996. Quantitative Immunohistchemistry of Factor VIII-Related Antigen in Breast Carcinoma. Amer.J.Clin. Pathol.105:705-10.

Knoerding, M.A., F. Steinberg, C. van Ackern, V. Budach, and C. Streffer. 1992. Vascular patterns of tumors: scanning and transmission electron microscopic studies on human xenografts. Strahlentherapie und Onkologie 168:444-52.

Konerding, M.A., A.J. Miodonski, and A. Lametschwandter. 1995. Microvascular Corrosion Casting in the Study of Tumor Vascularity: A Review. Scanning Microsc. 9:1233-44.

Kratky, R.G., C.M. Zeindler, D.K.C. Lo, and M.G. Roach. 1989. Quantitative Measurement from Vascular Casts. Scanning Microsc. 3:937-43.

Liotta, L. 1992. Cancer Cell Invasion and Metastasis. Sci. Am. 266,8:54-63.

Luscinskas, F.W., and J. Lawler. 1994. Integrins as dynamic regulators of vascular function. FASEB J. 8:929-938.

McCandless, J.R., A.E. Cress, I. Rabinovitz, C.M. Payne, G.T. Bowden, J.D. Knox, and R.B. Nagle. 1997. A human xenograft model for testing early events of epithelial neoplastic invasion. Intl. J. Oncology (in press).

Mickey, D.D., K.R. Stone, H. Wunderli, G.H. Mickey, and D.F. Paulson. 1980. Characterization of a human prostate adenocarcinoma cell line (DU145) as a moonolayer culture and as a solid tumor in athymic mice. p. 76-84. In Models for Prostate Cancer. G.P. Murphy (ed.) Alan R. Liss, Inc. New York.

Murphy, A.N., E.J. Unsworth, and W.G. Stetler-Stevenson. 1993. Tissue Inhibitor of Metalloproteinases-2 Inhibits bFGF-Induced Human Microvascular Endothelial Cell Proliferation. J. Cell. Phys. 157:351-358.

Nagle, R.B., M.K. Brawer, J. Kittelson, and V. Clark. 1991. Phenotypic relationships of prostatic intraepithelial neoplasia to invasive prostatic carcinoma. Amer. J. Pathol. 138:119-28.

Nagle, R.B., J. Hao, J.D. Knox, B.L. Dalkin, V. Clark, and A.E. Cress. 1995. Expression of Hemidesmosomal and Extracellular Matrix Proteins by Normal and Malignant Human Prostate Tissue. Amer. J. Pathol. 146:1498-507.

Rabinovitz, I., R.B. Nagle, and A.E. Cress. 1995. Integrin a6 expression in human prostate carcinoma cells is associated with a migratory and invasive phenotype in vitro and in vivo. Clin. Exp. Metastasis 13:481-91.

Rak, J.W., B.D. St. Croix, and R.S. Kerbel. 1995. Consequences of angiogenesis for tumor progression, metastasis, and cancer therapy. Anti-Cancer Drugs 6:3-18.

Senger, D.R. 1996. Molecular Framework for Angiogenesis. Amer. J. Pathol. 149:1-7.

Senger, D.R., S.R. Ledbetter, K.P. Claffey, A.P. Papadopoulos-Sergiou, C.A. Perruzzi, and M. Detmar. 1996b. Stimulation of Enothelial Cell Migration by Vascular Permeability Factor/Vascular Endothelial Growth Factor through Cooperative Mechanisms Involving the avb3 Integrin, Osteopontin, and Thrombin. Amer. J. Pathol. 149:293-305.

Shaw, L.M., and Mercurio, A.M. 1993. Regulation of alpha 6 beta 1 integrin laminin receptor function by the cytoplasmic domain of the alpha 6 subunit. J. Cell Biol. 123:1017-25.

Stracke, M.L., and L.A. Liotta. 1995. Molecular Mechanisms of Tumor Cell Metastasis. p. 233-247. In J. Mendelsohn, P.M. Howley, M.A. Israel, and L.A. Liotta (eds.), Molecular Basis of Cancer. W.B. Saunders Co., Philadelphia.

Vartanian, R.K., and N. Weidner. 1994. Correlation of Intratumoral Endothelial Cell Proliferation with Microvessel Density (Tumor Angiogenesis) and Tumor Cell Proliferation in Breast Carcinoma. Amer. J. Pathol. 144:1188-94.

Wakui, S., M. Furusato, T. Itoh, H. Sasaki, A. Akiyama, I. Kinoshita, K. Asano, T. Tokuda, S. Aizawa, and S. Ushigome. 1992. Tumour Angiogenesis in Prostatic Carcinoma Wtih and Withour Bone Marrow Metastasis: A Morphometric Study. J. Pathol. 168:257-262.

Waleh, N.S., M.D. Brody, M.A. Knapp, H.L. Mendonca, E.M. Lord, C.J. Koch, K.R. Laderoute, and R.M. Sutherland. 1995. Mapping of the Vascular Endothelial Growth Factor-producing Hypoxic Cells in Multicellular Tumor Spheroids Using a Hypoxia-specific Marker. Cancer Re. 55:6222-6226.

Weidner, N., J.P. Semple, W.R. Welch, and J. Folkman. 1991. Tumor Angiogenesis and Metastasis - Correlation in Invasive Breast Carcinoma. N. Engl. J. Med. 324:1-8.

Weidner, N., J. Folkman, F. Pozza, P. Bevilacqua, E. Allred, D. Moore, S. Meli, and G. Gasparini. 1992. Tumor angiogenesis: a new significant and independent prognostic indicator in early stage breast carcinoma. J. Natl. Cancer Inst. 84:1875-77.

Weidner, N., P.R. Carroll, J. Flax, Blumenfield, and J. Folkman. 1993. Tumor Angiogenesis Correlates with Metastasis in Invasive Prostate Carcinoma. Am. J. Pathol. 143:401-9.

Weidner, N. 1995. Intratumor Microvessel Density as a Prognostic Factor in Cancer. Amer. J. Pathol. 147:9-19.

Witkowski, C.M., I. Rabinovitz, R.B. Nagle, K.S. Affinito, and A.E., Cress. 1993. Characterization of integrin subunits, cellular adhesion and tumorigenicity of four human prostate cell lines. J. Cancer Res. Clin. Oncol. 119:637-44.

Zhang, H.-T., P. Craft, P.A.E. Scott, M. Ziche, H.A. Weich, A.L. Harris, and R. Bicknell. 1995. Enhancement of Tumor Growth and Vascular Density by Transfection of Vascular Endothelial Cell Growth Factor Into MCF-7 Human Breast Carcinoma Cells. J. Natl Cancer Inst. 87:213-219.